# **Endoscopic Light Scattering Spectroscopy for In Vivo Detection of Pre-Cancer in Bile Duct**

Le Qiu<sup>\*</sup>, Douglas K. Pleskow, Mandeep S. Sawhney, Paul K. Upputuri, Tyler M. Berzin, Mark F. Coughlan, Umar Khan, Xuejun Zhang, Jonah M. Cohen, Yuri N. Zakharov, Lei Zhang, and Lev T. Perelman

Center for Advanced Biomedical Imaging and Photonics, Beth Israel Deaconess Medical Center, Harvard University, Boston, USA

## **ABSTRACT**

Bile duct cancer, or cholangiocarcinoma, is a prevalent liver cancer often diagnosed at advanced stages, leading to poor survival rates. Therefore, the development of a reliable early detection technique is urgently needed. Current imaging techniques lack the necessary accuracy to distinguish between dysplastic and benign biliary ducts. Endoscopic techniques, while capable of directly assessing the bile duct lining, often suffer from insufficient sampling. In this paper we discuss a novel endoscopic optical light scattering technique designed to evaluate the malignant potential of the bile duct. The technique employs an ultraminiature spatial gating fiber optic probe compatible with cholangioscopes and endoscopic retrograde cholangiopancreatography (ERCP) catheters. The miniature optical probe enables the detailed investigation of the internal cellular composition of the bile duct epithelium using light scattering spectroscopy (LSS) and also allows for the assessment of the phenotypic properties of the underlying connective tissue with diffuse reflectance spectroscopy (DRS). In a pilot in vivo double-blind prospective study involving 29 patients undergoing routine ERCP procedures, the technique detected malignant transformation with 97% accuracy. Our pilot study suggests that biliary duct pre-cancer can be identified non-invasively in vivo, offering a promising new avenue for early detection and intervention in bile duct cancer.

**Keywords:** Pre-cancer, bile duct, light scattering spectroscopy, in vivo diagnosis

# 1. INTRODUCTION

Cholangiocarcinoma, more commonly referred to as bile duct cancer, is notoriously challenging to diagnose early due to its typically asymptomatic nature and the lack of identifiable risk factors in many patients [1,2] often leading to late-stage diagnosis and significantly hindering effective treatment options, resulting in poor patient outcomes [3]. The critical need for early detection methods, particularly for pre-cancerous conditions in the bile duct, is important [4,5]. Current diagnostic methods such as ultrasound, CT, MRCP, and PET-CT are utilized for cholangiocarcinoma detection. These techniques, however, generally suffer from low specificity and limited accuracy [6,7]. Endoscopic procedures provide a more direct approach to tissue evaluation and have improved sensitivity in detecting early tumor development. Techniques such as ERCP and advanced cholangioscopy, particularly with innovations like the SpyGlass cholangioscope, represent significant strides in diagnostic accuracy [8,9]. However, challenges remain, particularly due to the limited sampling capacity of brush cytology and small forceps biopsy.

Recent advancements have been made in refining diagnostic approaches. The use of narrow-band imaging (NBI) and probe-based confocal laser endomicroscopy (pCLE) has improved the visualization of mucosal changes. However, the effectiveness of these techniques in identifying pre-cancerous dysplasia is still under investigation [10,11]. Optical coherence tomography (OCT), offering high-resolution imaging of mucosal cross-sections, has demonstrated promise in enhancing detection rates of bile duct cancer, yet it requires considerable expertise in image interpretation [12,13].

In this study, light scattering spectroscopy (LSS) and diffuse reflectance spectroscopy (DRS) is applied to detect cholangiocarcinoma. The presented optical spectroscopic methods, which are operator-independent and compatible with small catheters, provide significant advantages in detecting structural and biochemical alterations in the epithelial lining of the bile duct. Our approach employs a custom designed miniature LSS-DRS fiber optic probe compatible with clinical

cholangioscopes and ERCP catheters, facilitating the in-depth investigation of the bile duct cellular composition and allowing early detection of malignancy.

# 2. METHODOLOGY

#### 2.1 Analysis of bile duct mucosa using DRS and LSS

DRS and LSS represent advanced non-invasive techniques for analyzing optical properties of the tissue, and are particularly useful in identifying early signs of malignancy in the bile duct mucosa. The techniques offer insight into the structural and biochemical characteristics of tissue, which are critical in the early detection of cholangiocarcinoma. In DRS, broadband light is projected onto the tissue surface, undergoing multiple elastic scattering and absorption events within the tissue matrix. The reflected light, carrying rich quantitative information about the tissue structure and composition, can then be analyzed. The steady-state spatially resolved diffusion theory serves as a fundamental model in analyzing and interpreting data obtained from diffuse reflectance spectroscopy (DRS). However, it faces limitations in accurately depicting small source-detector distances in anisotropic scattering mediums such as biological tissues. To address this, our group developed a phase function corrected diffusion theory to accurately extend the application of DRS to such challenging scenarios [14], which led to a refined expression for the case of small source-detector separations [15]:

$$R^{\text{ms}}(\rho,\lambda) \approx G(\lambda) \frac{\exp\left(-\sqrt{3}/2\,\mu_a \mu_t' \rho^2\right)}{\left(1 + {\mu_t'}^2 \,\rho^2\right)^{3/2}} \tag{1}$$

where  $G(\lambda) \approx \frac{\mu_s' \mu_t'}{10\pi} \exp\left(-\sqrt{\frac{3\mu_a}{\mu_t'}}\right)$ ,  $\mu'_t = \mu_a + \mu'_s$  is reduced transport coefficient,  $\mu_s'(\lambda) = \rho_s \sigma_s(\lambda)$  is the reduced

scattering coefficient, and  $\mu_a(\lambda) = c_{Hb} \left[ \alpha \, \varepsilon_{HbO_2}(\lambda) + (1-\alpha) \, \varepsilon_{Hb}(\lambda) \right]$  is the absorption coefficient. For the absorption coefficient,  $c_{Hb}$  is the total hemoglobin concentration,  $\alpha$  as the hemoglobin oxygen saturation parameter, and  $\varepsilon_{Hb}(\lambda)$  and  $\varepsilon_{HbO_2}(\lambda)$  are the respective wavelength dependent extinction coefficients of deoxygenated and oxygenated hemoglobin. The reduced scattering coefficient can be further approximated to  $\mu_s'(\lambda) = \rho_s \sigma_s(\lambda_0)(\lambda_0/\lambda)^r$  with the reduced scattering cross section  $\sigma_s(\lambda_0)$ , and scattering power  $\gamma$ . This model mainly focuses on reflectance due to multiple scattering and absorption in deeper tissue layers. By analyzing the reflectance given by equation (1), we can extract structural and biochemical insights, including total hemoglobin concentration, oxygen saturation, and effective scattering characteristics, which can give insights on the underlying mucosa conditions. However, it excludes the single backscattering events occurring in the superficial epithelial layer, which is often the initial site of dysplasia and malignancy.

Complimentary to DRS, LSS is crucial for assessing these single backscattering events in the epithelial layer. LSS effectively captures information pertinent to the malignant potential of the epithelium, employing a diagnostic parameter  $\Delta$ , previously utilized in Barrett's esophagus, pancreatic cysts and bile duct studies [15-17]. This parameter is a key component in evaluating the backscattering signal and determining the potential for malignancy in the epithelial layer. The single backscattering signal is isolated using spatial gating, leveraging the different dependencies of diffuse and single backscattering components on source-detector distance.

The custom DRS-LSS fiber optic probe provides two source-detector distances,  $120~\mu m$  and  $240~\mu m$ . At  $240~\mu m$  separation we observe a substantial reduction in the single backscattering component, allowing us to effectively disregard its influence on the backscattering signals [14]. The backscattering signals are then estimated using relationship

$$R^{\rm sb}(\lambda) \approx R^{\rm ex}(r_1, \lambda) - \xi R^{\rm ex}(r_2, \lambda) \tag{2}$$

where  $\xi$  is a coefficient determined via calibration procedure employing optical phantoms. This coefficient accounts for differences in multiple scattering signal strengths, which vary based on the source-detector distances. The approximation (2) is particularly accurate in the 600 to 800 nm wavelength range, where hemoglobin absorption could be neglected.

From here the diagnostic parameter  $\Delta = \frac{1}{2} \sum_{\lambda} \left( \overline{R}^{\text{sb}} \left( \lambda \right) - \langle \overline{R}^{\text{sb}} \left( \lambda \right) \rangle \right)^2$  can be calculated using the normalized and the root-

mean-square–normalized single backscattering components summed across all spectral points λ [15-17].

## 2.2 Design and Implementation of the Clinical LSS-DRS Fiber Optic System

The clinical setup utilized a 75 W fiber-coupled xenon short arc light source (SLS205, Thorlabs) for white light illumination, and featured three spectrometers (AvaSpec-2048-USB2, Avantes) to collect spectra at three different source-detector separations. The entire system was mounted on a mobile cart for easy transportation within the clinic. A custom-built, spatially gated LSS-DRS fiber optic probe facilitated the light delivery and collection. A MATLAB-based custom graphical user interface (GUI) was developed for system operation and data acquisition. The probe design incorporated seven fibers, each with a core diameter of 100  $\mu$ m and a numerical aperture (NA) of 0.22. Spatial gating LSS is accomplished by using a single outer-ring fiber for light delivery and three fibers positioned at distances of 120  $\mu$ m, 220  $\mu$ m, and 240  $\mu$ m from the delivery fiber, used for light collection. Each collection fiber was connected to a separate spectrometer channel. For this study, we employed only two collection fibers at 120  $\mu$ m and 240  $\mu$ m source-detector separations. The probe diameter was 0.9 mm, ensuring compatibility with the 1.2 mm working channel of all standard cholangioscopy systems and ERCP catheters.

# 2.3 In Vivo Clinical LSS-DRS Measurement during ERCP Procedures

In vivo clinical LSS-DRS measurements were conducted during routine ERCP procedures on 29 subjects suspected of having dysplasia and malignancy in the bile duct. These subjects, initially screened and referred by other institutions to the BIDMC Center for Advanced Endoscopy Center, underwent the procedures after understanding and consenting to the process and potential complications. The BIDMC Institutional Review Board reviewed and approved the protocol. During the ERCP procedures, patients were either lying on their back or side on an X-ray table. An endoscope was inserted into the esophagus, through the stomach, and into the duodenum. A video feed from the endoscope camera displayed on a screen above the table aided the examination. Air was pumped through the endoscope to inflate the stomach and duodenum for better visibility. Upon locating the duodenal papilla, a sphincterotome, a curved catheter with a cutting wire, was guided through the endoscope into the papilla (Fig. 1).

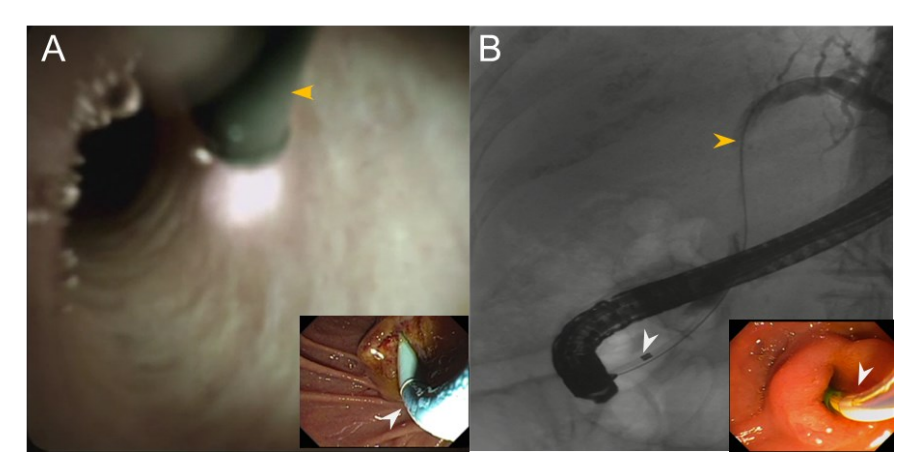


**Figure 1. In vivo LSS-DRS measurement process in the bile duct using cholangioscopy and ERCP catheter.** (A) Image of the LSS-DRS fiber probe (indicated by a white arrow) as seen through a cholangioscope. The probe targets a specific site within the bile duct epithelial lining for spectral data acquisition. Inset: A view of the cholangioscope entry into the pancreaticobiliary system via the ampulla of vater, as observed through a duodenoscope. (B) X-ray visualization showing the ERCP catheter, which houses the LSS-DRS fiber probe, being maneuvered into the pancreaticobiliary system. The ERCP guidewire, highlighted with an orange arrow, reaches into the intrahepatic duct. A radiopaque band at the ERCP catheter distal end (white arrow) serves as a reference for the precise placement of the LSS-DRS fiber probe.

Dye injection into the ducts provided X-ray contrast for visualizing the ductal tree and identifying any blockages or narrowing areas. The cholangioscope or ERCP catheter, inserted through the duodenoscope, allowed for direct viewing of the bile duct and fiber probe access. Spectra were automatically acquired when the LSS-DRS fiber probe was near and

approximately to the bile duct wall. X-ray images and cholangioscope videos were recorded for site identification during data collection, which lasted under two minutes per patient, including probe insertion, spectral collection at 2 to 14 sites, and probe removal. Biopsies were collected from several sites for pathological examination, following standard care. In cases where only brush cytology was performed, spectra were obtained at each site before the procedure. The size of LSS-DRS measurements, roughly  $100 \mu m$  to  $200 \mu m$ , matched the microscopic field of view used for pathology-based diagnosis. Throughout the procedures, no adverse events were observed.

## 3. RESULTS

In vivo spectra were obtained with the LSS-DRS probe from various bile duct sites, including high-grade dysplasia, low-grade dysplasia, inflammation, and benign areas. These spectra correspond to measurements taken at source-detector distances of 120  $\mu$ m and 240  $\mu$ m, showing excellent fits with the DRS model [15]. An inverse DRS algorithm based on equation (1) was developed to fit spectra (500 nm to 800 nm range) taken at source-detector distances of 120  $\mu$ m and 240  $\mu$ m, to extract key parameters such as hemoglobin concentration, oxygen saturation, and scattering power for the underlying connective tissue at each site. This analysis encompassed 53 benign sites (BNG), 49 inflamed sites (INF), nine low-grade dysplasia sites (LGD), and 50 sites of high-grade dysplasia (HGD) or early cancer (CAN). Figure 2 presents a summary of all the measurement results.

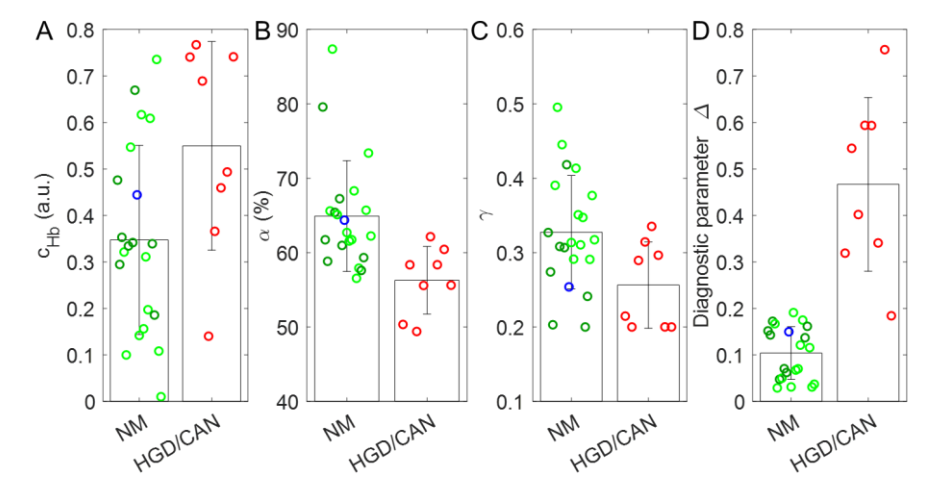


Figure 2: Tissue parameters reconstructed from bile duct in vivo spectroscopic data. Each circle in the diagram represents the extreme values (either highest or lowest) from all measurement sites for each subject, color-coded to indicate the pathological condition of the bile duct: red for high-grade dysplasia or cancer, blue for low-grade dysplasia, green for benign sites with inflammation, and bright green for benign sites. The height of each bar indicates the average value of these points, with error bars illustrating the standard deviation. The panels show DRS-based measurements of (A) the highest hemoglobin concentration ( $c_{Hb}$ ), (B) the lowest oxygen saturation ( $a_{Hb}$ ), (C) the lowest scattering power ( $a_{Hb}$ ), and (D) the LSS-based highest diagnostic parameter ( $a_{Hb}$ ). NM: nonmalignant, HGD: high grade dysplasia, CAN: cancer

Since measurements were taken at sites of varying pathological conditions for each subject, ranging from nonmalignant to potentially malignant, the figure displays only the extreme values (the highest or the lowest). Angiogenesis, the process of new blood vessel formation that sustains malignant cells, plays a crucial role in the development of neoplasia [18]. This process often results in increased hemoglobin concentration, a hallmark of advanced malignancy stages. Therefore, we focused on the highest hemoglobin concentration ( $c_{Hb}$ ) recorded for each subject, as shown in Fig. 2A. A similar rationale applies to oxygen saturation that tumor growth leads to rapid oxygen consumption by proliferating cells, creating a hypoxic environment [19]. Thus, the lowest oxygen saturation values are of particular interest. Regarding the DRS-based scattering power ( $\gamma$ ), earlier studies suggest that malignant tissues often display a less steep slope in the DRS spectrum [20], which typically correlates with a reduction in the value of  $\gamma$ . We plotted only the lowest  $\gamma$  values for each subject. While the above-mentioned trends are observable in comparing nonmalignant bile ducts (including benign, inflammation, and low-grade dysplasia) with malignant sites (Fig. 2A-C), as indicated by the height of the bars, there are significant overlaps in individual results, complicating their use in definitive diagnosis. The overlaps may be attributed to the later-stage development of angiogenesis and hypoxic environments in malignancy. Regarding scattering power, the

bile duct wall beneath the thin epithelial lining comprises muscle and dense fibrous tissue in the fibromuscular layer. As these components do not undergo significant changes in the early stages of malignant transformation, the subepithelial scattering power derived from DRS data is likely not highly sensitive to early malignancy detection.

The single backscattering component, primarily influenced by epithelial scattering, can be extracted from spatially gated reflectance data in the 600 nm to 800 nm range. This process, detailed in the Methods section, allowed us to reconstruct single backscattering components which were used to calculate diagnostic parameter  $\Delta$ , which was previously demonstrated to indicate epithelial nuclear size distribution [22]. Figure 2D showed the highest diagnostic parameter  $\Delta$  for each enrolled subject, which almost perfectly separates nonmalignant subjects from HGD and cancer subjects. We employed the predetermined diagnostic cutoff for the LSS diagnostic parameter  $\Delta$ , established previously in pancreatic cyst studies [17]. The use of the same diagnostic cutoff can be justified by taking into account similarities in the epithelial lining of the bile duct and mucinous pancreatic cysts. Malignancy classification based only on the LSS diagnostic parameter (Fig. 2D) gives a sensitivity of 88% (95% CI: 53–99%) and a specificity of 100% (95% CI: 85–100%), a significant improvement over the standard of care ERCP-based diagnosis. This could be expected given that the LSS signal is dominated by the scattering in the epithelial lining, where most malignant transformations occur.

## 4. CONCLUSIONS

In summary, this study introduces a minimally invasive and effective optical spectroscopic method capable of accurately detecting pre-cancerous and early cancerous changes in the biliary duct non-invasively. The primary advantage of this technique is the miniaturized spatial gating fiber optic probe, which is cost-effective and ensures a seamless fit within the narrow spaces of cholangioscopes and ERCP catheters, making it practical for clinical use. Given that approximately half a million ERCP procedures are conducted yearly in the United States using standard ERCP catheters [23], this technique's compatibility with both conventional ERCP catheters and cholangioscopes significantly broadens its applicability. In our study, clinicians chose between conventional ERCP catheters and cholangioscopes based on clinical necessity, independent of study requirements, with no impact on the procedure or outcomes of the LSS-DRS measurements. Notably, clinicians do not require additional training to use this system, as it operates automatically, and the probe placement is similar to standard biopsy forceps. Our pilot study, involving 29 patients undergoing routine ERCP procedures, demonstrated the method's efficacy in detecting subtle epithelial changes indicative of pre-cancerous and cancerous conditions in the bile duct. The optical measurements are quickly completed within two minutes, underscoring the technique's potential as a valuable tool for early dysplasia detection in the bile duct.

## ACKNOWLEDGMENTS

This work was supported by US National Institutes of Health grants R01 EB025173, R01 CA228029, and R01 CA218382 and US National Science Foundation grants EFRI-1830878, CBET-1948722, CBET-2220273, and CBET-2325317.

## REFERENCES

- [1] Blechacz, B., Komuta, M., Roskams, T., and Gores, G. J., "Clinical diagnosis and staging of cholangiocarcinoma," Nat. Rev. Gastroenterol. Hepatol. 8, 512-522 (2011).
- [2] Razumilava, N., and Gores, G. J., "Cholangiocarcinoma," Lancet 383, 2168-2179 (2014).
- [3] Bridgewater, J., Galle, P. R., Khan, S. A., Llovet, J. M., Park, J. W., Patel, T., Pawlik, T. M., and Gores, G. J., "Guidelines for the diagnosis and management of intrahepatic cholangiocarcinoma," J. Hepatol. 60, 1268-1289 (2014).
- [4] Nakeeb, A., Pitt, H. A., Sohn, T. A., Coleman, J., Abrams, R. A., Piantadosi, S., Hruban, R. H., Lillemoe, K. D., Yeo, C. J., and Cameron, J. L., "Cholangiocarcinoma: A spectrum of intrahepatic, perihilar, and distal tumors," Ann. Surg. 224, 463-475 (1996).
- [5] Fleming, K. A., Boberg, K. M., Glaumann, H., Bergquist, A., Smith, D., and Clausen, O. P. F., "Biliary dysplasia as a marker of cholangiocarcinoma in primary sclerosing cholangitis," J. Hepatol. 34, 360-365 (2001).

- [6] Rizvi, S., Khan, S. A., Hallemeier, C. L., Kelley, R. K., and Gores, G. J., "Cholangiocarcinoma evolving concepts and therapeutic strategies," Nat. Rev. Clin. Oncol. 15, 95-111 (2018).
- [7] Aljiffry, M., Abdulelah, A., Walsh, M., Peltekian, K., Alwayn, I., and Molinari, M., "Evidence-based approach to cholangiocarcinoma: a systematic review of the current literature," J. Am. Coll. Surg. 208, 134-147 (2009).
- [8] Chen, Y. K., and Pleskow, D. K., "SpyGlass single-operator peroral cholangiopancreatoscopy system for the diagnosis and therapy of bile-duct disorders: a clinical feasibility study (with video)," Gastrointest. Endosc. 65, 832-841 (2007).
- [9] Draganov, P. V., Chauhan, S., Wagh, M. S., Gupte, A. R., Lin, T., Hou, W., and Forsmark, C. E., "Diagnostic accuracy of conventional and cholangioscopy-guided sampling of indeterminate biliary lesions at the time of ERCP: a prospective, long-term follow-up study," Gastrointest. Endosc. 75, 347-353 (2012).
- [10] Itoi, T., Sofuni, A., Itokawa, F., Tsuchiya, T., Kurihara, T., Ishii, K., Tsuji, S., Moriyasu, F., and Gotoda, T., "Peroral cholangioscopic diagnosis of biliary-tract diseases by using narrow-band imaging (with videos)," Gastrointest. Endosc. 66, 730-736 (2007).
- [11] Wang, K. K., Carr-Locke, D. L., Singh, S. K., Neumann, H., Bertani, H., Galmiche, J.-P., Arsenescu, R. I., Caillol, F., Chang, K. J., Chaussade, S., Coron, E., Costamagna, G., Dlugosz, A., Ian Gan, S., Giovannini, M., Gress, F. G., Haluszka, O., Ho, K. Y., Kahaleh, M., Konda, V. J., Prat, F., Shah, R. J., Sharma, P., Slivka, A., Wolfsen, H. C., and Zfass, A., "Use of probe-based confocal laser endomicroscopy (pCLE) in gastrointestinal applications. A consensus report based on clinical evidence," United European Gastroenterol. J. 3, 230-254 (2015).
- [12] Poneros, J. M., Tearney, G. J., Shiskov, M., Kelsey, P. B., Lauwers, G. Y., Nishioka, N. S., and Bouma, B. E., "Optical coherence tomography of the biliary tree during ERCP," Gastrointest. Endosc. 55, 84-88 (2002).
- [13] Corral, J. E., Mousa, O. Y., Krishna, M., Levink, I. J. M., Pursell, K. R., Afsh, M., Kroner, P. T., Harnois, D. M., Wolfsen, H. C., Wallace, M. B., and Lukens, F. J., "Volumetric laser endomicroscopy in the biliary and pancreatic ducts: a feasibility study with histological correlation," Endoscopy 50, 1089-1094 (2018).
- [14] Vitkin, E., Turzhitsky, V., Qiu, L., Guo, L., Itzkan, I., Hanlon, E. B., and Perelman, L. T., "Photon diffusion near the point-of-entry in anisotropically scattering turbid media," Nat. Commun. 2, 587 (2011).
- [15] Pleskow, D. K., Sawhney, M. S., Upputuri, P. K., Berzin, T. M., Coughlan, M. F., Khan, U., Glyavina, M., Zhang, X., Chen, L., Sheil, C. J., and Cohen, J. M., "In vivo detection of bile duct pre-cancer with endoscopic light scattering spectroscopy," Nat. Commun. 14(1), 109 (2023 Jan 7).
- [16] Qiu, L., Pleskow, D. K., Chuttani, R., Vitkin, E., Leyden, J., Ozden, N., Itani, S., Guo, L., Sacks, A., Goldsmith, J. D., Modell, M. D., Hanlon, E. B., Itzkan, I., and Perelman, L. T., "Multispectral scanning during endoscopy guides biopsy of dysplasia in Barrett's esophagus," Nat. Med. 16, 603-606 (2010).
- [17] Zhang, L., Pleskow, D. K., Turzhitsky, V., Yee, E. U., Berzin, T. M., Sawhney, M., Shinagare, S., Vitkin, E., Zakharov, Y., Khan, U., Wang, F., Goldsmith, J. D., Goldberg, S., Chuttani, R., Itzkan, I., Qiu, L., and Perelman, L. T., "Light scattering spectroscopy identifies the malignant potential of pancreatic cysts during endoscopy," Nat. Biomed. Eng. 1, 1-7 (2017).
- [18] Pugh, C. W. and Ratcliffe, P. J., "Regulation of angiogenesis by hypoxia: role of the HIF system," Nat. Med. 9, 677-684 (2003).
- [19] Nishihara, K., Hori, K., Saito, T., Omori, T., Sunakawa, H., Minamide, T., Suyama, M., Yamamoto, Y., Yoda, Y., Shinmura, K., Ikematsu, H., and Yano, T., "A study of evaluating specific tissue oxygen saturation values of gastrointestinal tumors by removing adherent substances in oxygen saturation imaging," PLoS One 16, e0243165 (2021).
- [20] Zonios, G., Perelman, L. T., Backman, V., Manoharan, R., Fitzmaurice, M., Van Dam, J., and Feld, M. S., "Diffuse reflectance spectroscopy of human adenomatous colon polyps in vivo," Appl. Opt. 38(31), 6628-6637 (1999).
- [21] Hong, S. M., Kang, G. H., Lee, H. Y., and Ro, J. Y., "Smooth muscle distribution in the extrahepatic bile duct: histologic and immunohistochemical studies of 122 cases," Am. J. Surg. Pathol. 24, 660-667 (2000).
- [22] Qiu, L., Chuttani, R., Pleskow, D. K., Turzhitsky, V., Khan, U., Zakharov, Y. N., Zhang, L., Berzin, T. M., Yee, E. U., Sawhney, M. S., Li, Y., Vitkin, E., Goldsmith, J. D., Itzkan, I., and Perelman, L. T., "Multispectral light scattering endoscopic imaging of esophageal precancer," Light Sci. Appl. 7, 17174 (2018).
- [23] Cappell, M. S. and Friedel, D. M., "Stricter national standards are required for credentialing of endoscopic-retrograde-cholangiopancreatography in the United States," World J. Gastroenterol. 25, 3468-3483 (2019).